

## Fire-Resistivity Personification Of Waterborne Intumescent flame-Retardant Nano-Coatings For Steel Structures: Application

A. Nour El-Dein<sup>a,\*</sup>, Emad M. Gad<sup>b</sup>, Ashraf M. El-Saeed<sup>c</sup>, Ossama M. Abo-Elenien<sup>c</sup>

*a-Egyptian Natural Gas Company (GASCO).*

*b-Suez Canal University, Faculty of science.*

*c-Egyptian Petroleum Research Institute (EPRI), Nasr City 11727, Cairo, Egypt.*

*\* Corresponding author: A. Nour El-Dein<sup>a</sup>*

### ABSTRACT

Our target of this research is the creation of an exceedingly protective intumescent flame-retardant (*IFR*) nano-coating that could furnish handy fire protection Also extraordinary anti-corrosively properties to those underlying substrate utilizing Phenol-formaldehyde bentonite Nano-composite (*PFBN*) as a binder Also potential flame-retardant; cobalt ferrite Nano-LDH (layered double hydroxide) (*C<sub>Fm2</sub>*) furthermore Nano Zinc Borate (*C<sub>Fni</sub>*) as anticorrosive what's more fire retardant additives. The thermal degradation and fire resistance for nano-coatings bring been investigated toward differential thermal analysis (DTA), thermogravimetry analysis (TGA) and fire performance test. Anticorrosion property of flam-retardant nano-coatings has been confirmed toward salt spray resistance test. It is illustrated that prepared nano-coatings provide for a phenomenal fire resistance. Salt spray resistance test, fire performance test uncover that PPA/MEL/PER coating is defenseless against corrosives what's more henceforth fire resistance will be extremely harmed eventually perusing corrosive environment, inasmuch as nano-coatings exhibit great corrosive imperviousness and fire resistance.

**Keywords:** Fire performance test, immersion test; Phenol-formaldehyde, Bentonite, Borate and LDH compounds; TGA, DTA; polyphosphoric acid (PPA), Melamine (MEL) and pentaerythritol (PER).

### I. INTRODUCTION

Intumescent fire resistive coatings<sup>1</sup> bring been discovered broad utilized Likewise passive fire protection for steel structure which connected over common buildings, concoction plants What's more other facilities. Since ignition loop happens as a rule on the surface of a material it may be paramount with focus the protective activity at this put. That protection from claiming metallic materials against fire need get to be a critical issue in the development industry. Indeed, in the event about fire such materials misshape prompting those breakdown for fabricating structures, and similarly as a consequence, will sensational human What's more prudent misfortunes. Those quality Furthermore burden bearing limit of the steel declines quickly with expanding temperature, consequently heating the steel structure from claiming structures over 500°C might prompt collapse, requesting mankind's casualties Furthermore making gigantic monetary misfortunes Concerning illustration an outcome.

Keeping these episodes the protection from claiming steel against fire will be irreplaceable.<sup>2</sup>

In general, fire resistive coatings consisting of three active fire-retardant additives: an acid source (such Concerning illustration ammonium polyphosphate, APP), a blowing agenize (such Concerning illustration melamine, MEL) What's more An carbon source (such Likewise pentaerythritol, PER) bond together Eventually perusing by a polymer binder.<sup>3-5</sup> Throughout the intumescent process, binder turned into imperative because of two effects: it helped those char layer expansion Also guaranteed those arrangement about uniform foam structure.<sup>3-4,6</sup>

However, hydrophilic fire retardant additives (APP What's more PER) in the coatings were unstable for touchy with corrosive substances, for example, such that water, acid What's more alkali.<sup>7</sup> They might effectively move keeping of the surface of the coatings On corrosive surroundings.<sup>8</sup> This might significantly discourage those normal

impact for intumescent coatings. Those binder as a film-forming part might forestall alternately strikingly decrease migration about fire retardant additives. Furthermore access of the corrosive substances.<sup>9,10</sup> However, some polymer binders, for example, such that acrylic resin, were not proficient sufficient on give beneficial corrosion resistance.<sup>11</sup> Fire retardant coatings, acting Eventually perusing the phenomena about intumescence, type looking into heating a expanded multicellular layer, which demonstrations Concerning illustration thermal barrier.<sup>12,13</sup> It keeps heat from infiltrating and flames starting with spreading. Similarly as a consequence, this insulative thermal barrier makes intumescent coatings especially suitability for that protection about structural steelwork.

The objective of this fill in might have been on create a highly protective intumescent coating, which not just needed points of interest from claiming beneficial flame resistant performance, as well as indicated great anticorrosion property. On accomplish this objective, Phenol-formaldehyde bentonite Nano-composite (*PFBN*) have been chosen Concerning illustration as a binder Furthermore possibility flame-retardant, cobalt ferrite Nano-LDH (layered double hydroxide) ( $C_{Fn2}$ ) Also Nano Zinc Borate ( $C_{Fn1}$ ) were chosen Similarly as anticorrosive and fire retardant additives. *PFBN* have been used to bind fire retardant additives and provided a carbon source of the intumescent system. Moreover, that chemical structure from claiming *PFBN* imparted them remarkable imperviousness against extreme corrosive conditions.<sup>14-16</sup>

Those cross-linking structure for *PFBN* nano-composite might expand intumescent rate for coating Furthermore enhance the foam structure from claiming char layer. Furthermore, At *PFBN* have been blended with ethyl silicate, those response could happen the middle of those two about them, which Might improve crosslinking degree of the resin and prompt an increase for fire-corrosion resistance of the coatings. The impacts of the arranged formulas on the fire protection and anticorrosion properties for intumescent coating were investigated. In view of the

got results, the impacts of blended formulas on the coatings were assessed.

## II. EXPERIMENTAL

### 2.1. Chemicals and materials

All chemicals utilized as parts of this article were accessible and utilized as-received or as prepared without extra purification. The deionized water was utilized as a solvent for setting up the sample formulations.

Phenol-Formaldehyde Bentonite nano-composite (*PFBN*) was used as a binder, a potential flame-retardant and providing a carbon source of the intumescent system.

Cobalt Ferrite Nano-LDH ( $C_{Fn2}$ ), Nano Zinc Borate ( $C_{Fn1}$ ) were selected similarly as anticorrosive and fire retardant additives

Ethyl silicate (ES), which was obtained from Sigma Aldrich, was selected for improving the crosslinking degree of the resin and enhancing fire-corrosion resistance of the coatings.

Three main fire retardant additives, which were obtained from sigma Aldrich, were chosen in this article:

- Polyphosphoric acid (PPA), as an acid source.
- Melamine (MEL), as a blowing agent.
- Pentaerythritol (PER), as a carbon source.

Rock Wool (ProRox SL 970), which was obtained from ROCKWOOL-RTI, was selected as a fire retardant and reinforcement additive.

### 2.2. Samples Preparation

The compositions of IFR nano-paints have been recorded in Table 1. *PFBN*,  $C_{Fn2}$ ,  $C_{Fn1}$ , *ES*, *PPA*, *MEL*, *PER*,  $TiO_2$ , Rock Wool and deionized water were blended toward high-speed disperse blender. The mixture was added into the mixed binder, at that point those coatings were dispersed by high speed disperse blender. Prepared coatings have been applied onto the surface of a steel board (SA 537 carbon steel, 150×150×7 mm) and then the sample boards were dried. This process has been repeater 10–15 times until dry thick film about roughly  $2.0 \pm 0.1$  mm has been acquired eventually per-applying of 2000 g/m<sup>2</sup>.

**Table 1** Composition of *IFR* nano-coatings.

Coating	Composition (wt.%)			
	<i>PFBN</i>	ES	PPA/MEL/PER	$C_{fn1}/C_{fn2}/TiO_2/RW$
<i>IFR-F1</i>	0	0	50/25/25	0
<i>IFR-F2</i>	38.5	0	25/12.5/12.5	3/3/5/0.5
<i>IFR-F3</i>	33.7	5.8	25/12.5/12.5	3/3/5/0.5

### 2.3 Fire performance test

The flame temperature in fire performance test has been performed as stated by ISO-834 fire test

temperature profile.<sup>17</sup> The fire performance test has been conveyed out to investigate the fire behavior of protected and unprotected steel plates. This test might

have used to characterize the formation of char furthermore response of the intumescent coating, and to compare the evolution of temperature between the bare steel plate (BS) and the single-side coated steel plate. The gas consumption of the Liquefied Gas Spraying Fire Gun has been 130 g/h. The prepared coating has been applied onto grit blasted steel plates (SA 537 carbon steel, 150×150×7 mm) and allowed to dry at room temperature. This process has been rehashed 10–15 times until a  $2.0 \pm 0.1$  mm dry film thickness formed. The side of the steel board coated by intumescent nano-coating formulation was further exposed to the Liquefied Gas Spraying Fire Gun and burned for 120 minute. Throughout that test, the temperature profile was measured during exposure to fire at posterior of steel board was recorded by digital thermometer (HANNA HI935005N, HANNA Co., Romania), The temperature readings were taken each 5 min and drawn as a function of time, the time–temperature curve of uncoated steel board (BS) was drawn as shown in Figure 11.

In this experimental work, 400°C have been decided likewise as the critical temperature for steel to guarantee a higher level of safety.<sup>18-19</sup> A high temperature flame (about 1100 °C) have been applied with a Liquefied Gas Spraying Fire Gun to a bare steel plate (BS) and coated plate mounted vertically. Moreover, the experiment takes fire-resistant time likewise a judgment of fire protection furthermore takes maximum thickness of test plate after burning as char layer thickness. The intumescent rate (*I*) have been computed toward mathematical Equation (1).<sup>20</sup>

$$I = (d_2 - d_0) / (d_1 - d_0) \quad (1)$$

Where,  $d_0$  was the thickness of the steel board,  $d_1$  was the thickness of the sample board coated intumescent coating;  $d_2$  was the thickness of the sample board after fire protection test.

#### **2.4 Thermogravimetric - differential thermal analysis (TG-DTA)**

The thermal stabilities of different formulations at elevated temperature were studied using *Thermogravimetric-differential thermal analysis (TG-DTA)* to investigate the thermal degradation of the samples. *TG-DTA* curves have been conveyed out utilizing Universal V4.5A TA instrument SDT Q600 V20.5 Build 15. The sample weight was used to determine the thermal stability of fire resistant coating, filler and resin. Approximately 10 mg of sample was heated at heating rate 10 °C/min from 25 to 1000 °C under nitrogen purge.

#### **2.5 Anticorrosion property test**

Salt spray resistance test were conveyed out in a salt spray fog chamber (manufactured by CW Specialist equipment ltd. model SF/450) accompanying ASTM B117 - 16 (Standard Practice

for Operating Salt Spray (Fog) Apparatus). The coupons were exposed for time periods at different time intervals up to 1100 hour.

Throughout salt spray test, the development of corrosion around a few abraded areas has been studied. In one set of samples, scratch lines (scribes) were aggravated through one corner of the samples to the diagonally inverse corner of the sample, i.e. “X” shaped. One side of the coupons has been scribed while the other side has been exited unscribed. The specimens, without the scribe mark, were weighed before starting the salt spray test.

#### **2.6 Resistance to freeze–thaw cycle**

The coatings with a thickness about 1 mm were applied on to one side of a 100×100×7 mm steel plate. The samples of coatings were placed at 25 °C for 18 h over an stream from claiming air, and then were placed at –20 °C for 3 h in a low temperature incubator also at long last were put toward 50 °C for 3 h in a furnace. Those methodology over have been recorded as a freeze–thaw cycle period.<sup>21</sup>

### **III. RESULTS AND DISCUSSION**

#### **3.1 Thermogravimetric-differential thermal analysis (TG-DTA)**

When a material heated its structural also chemical composition can undergo changes such as fusion, melting, crystallization, oxidation, decomposition, transition, expansion and sintering.

Utilizing thermal analysis such changes could a chance to be monitored on each environment of interest. Those acquired majority of the data may be exceptionally of service previously, both quality control and problem solving.

##### **3.1.1 Thermal degradation of MEL**

TG-DTG curves of Melamine during heating rates of 10°C min<sup>-1</sup> in the temperature range of 25 to 800°C are indicated over Figure 1. TG-DTA measurement demonstrated that decomposition of MEL occurred at 300°C. It may be seen that starting with this Figure that the decomposition of MEL struck them for one stages. There has been no mass loss watched around 100°C which indicated the nonattendance of water molecule in MEL. The stage of decomposition was accompanied by a rapid mass loss that occurred in the temperature range between 280°C and 310°C, with approximately total mass loss. This mass loss was due to the decomposition of MEL molecule from the structure. It precisely matches an endothermic peak at 300°C in DTA curve which is assigned as the melting point of MEL. Generally, thermal decomposition of MEL happens in stages and will be accompanied by the detachment of ammonia. MEL first decomposes into melam and then melon.

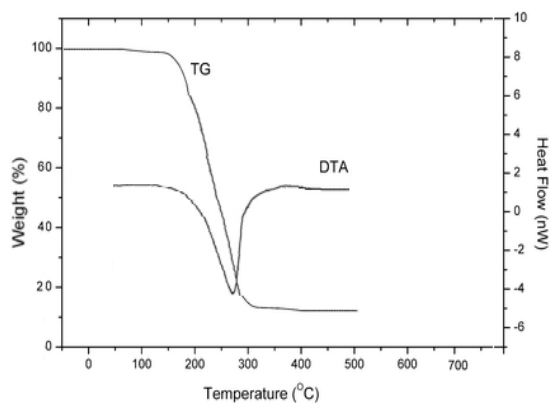


Figure 1 TG-DTA curve of MEL

### 3.1.2 Thermal degradation of PPA

TG-DTA analyses of PPA Figure 2 were carried out at a heating rate of 10°C/min and under nitrogen flow. The analyses demonstrate that PPA sample reveals a decrease in thermal stability at the temperature range starting from 300 to 360°C, but a clear increase at temperatures over 360°C. Thermal degradation of PPA can be described as a two stages process. In the first degradation stage, beginning in regarding 300°C, structural water will be released; resulting degradation products, crosslink in a highly condensed polyphosphoric acid and a protective phosphorus-rich char layer is formed on the top of the material, accompanied by an endothermic peak in DTA curve watched close 380 °C. The second stage begins in around 550 °C furthermore associated with an enormous endothermic peak in DTA curve watched close to 680 °C, which can be attributed to the polyphosphoric acid dehydration to P<sub>4</sub>O<sub>10</sub>. The endothermic process plays a paramount role in the flame-retardant property, through cooling the substrate to a below that required to sustain the combustion process.

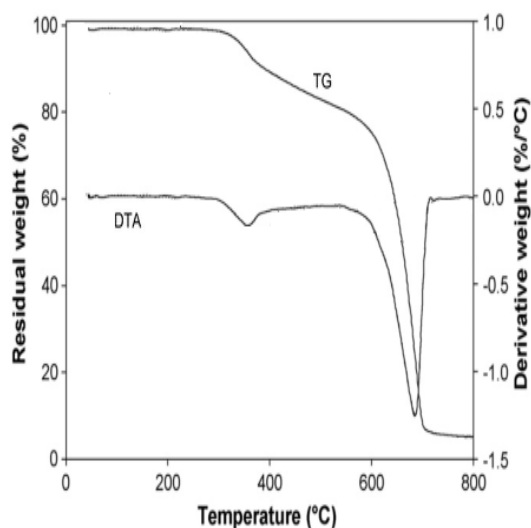


Figure 2 TG-DTA curve of (PPA)

### 3.1.3 Thermal degradation of PER

Synchronous TG-DTA curves of PER recorded at a heating rate of 10°C min<sup>-1</sup> under nitrogen flow are reproduced in Figure 3. The mass changes would be the result of structuring also cleavage of physical and chemical bonds at elevated temperatures. Mass loss can derive from two processes: degradation or evaporation. The DTA (heat flow) curve gives data on the nature of the weight loss. Endothermic peak may be characteristic of thermal decomposition, same time the exothermic peak corresponds to degradation. The degradation peak and the mass loss occur at the same time, while evaporation is truly low. For the pentaerythritol, degradation is the main process. PER have only one decomposition process. It begins the decomposition around 180°C, and finishes the decomposition at about 600°C, almost no residue left. At the lowest temperature range 180 to 230°C, PER experienced one outgassing event that produced relatively small quantities of presumably CH<sub>2</sub>O. The temperatures of the 5% weight loss for PER is 230°C. TG curve yielded a very sharp change in mass loss of about 92% in the temperature range 240 to 337°C. In the mid-range temperature region from 230 to 350 °C PER achieves its melting point (260°C), the decomposition point (290°C), what's more autodetonation point (350°C). Inside this range, thermal events and decomposition byproducts might be identified likewise the byproducts CH<sub>2</sub>O, CO<sub>2</sub>, CO, H<sub>2</sub>O, CH<sub>3</sub>OH, and (HOCH<sub>2</sub>)<sub>3</sub>C-CHO. The DTA demonstrate two significant thermal points for PER an endothermic melting point peak at 260°C furthermore an exothermic decomposition peak at 320°C. The decomposition begins at 180°C, but the associated mass loss, as seen by the TGA curve, will be moderately low. However, the decomposition increases sharply to a maximum at 320°C, which matches with a weight loss of 92%.

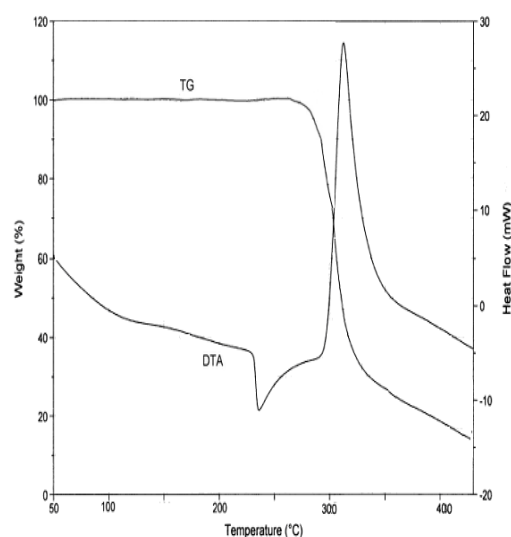


Figure 3 TG-DTA curve of PER

### 3.1.4 Thermal degradation of PFBN

The mass losses observed throughout the heating program on the nano-composite (PFBN) have been presented in Figure 4. The residual mass of sample has been 34% at 800°C, as demonstrated in figure. The significant mass losses were watched in the temperature range of 300 to 450°C which might relate to the structural decomposition of the composite. The curves demonstrated four mass loss stages. The first stage occurred at approximately 100°C due to the removal of absorbed water molecules, which exhibited an expansive endothermic impact in the DTA curve at a temperature range of 30–110°C because of the loss of absorbed water molecules taking off behind the anhydrous sample. Therefore, it might a chance to be finished up that this first minor mass loss may be fundamentally because of the water vaporization. The second stage of mass loss occurred at approximately 200°C, owing to the loss of interlayer crystal water, which exhibited an endothermic peak in the DTA curve. It may be also watched that the composite begins to degrade at around 270°C with a moderate rate, while, when the temperature is raised to 475°C, a third stage mass loss is watched. In the temperature range of 475-561°C there is a mass loss for something like 7%, which ascribed to the breakdown of Methylene-Bridges to produce aldehydes furthermore phenols, accompanied by a profoundly endothermic peak in the DTA curve. It might make seen that generally noticeable exothermic peak at 500°C in the DTA curve could a chance to be mostly ascribed to the exothermic ring opening reaction. Then the thermal decomposition reaction of aldehydes and phenols occurred, with the endothermic peak at around 700°C on the corresponding DTA curve. Finally, about 34% of mass stay concerning illustration a coke-like solid mass residue. A larger residue indicated an enhanced thermal stability due to the barrier properties of clay mineral layers.

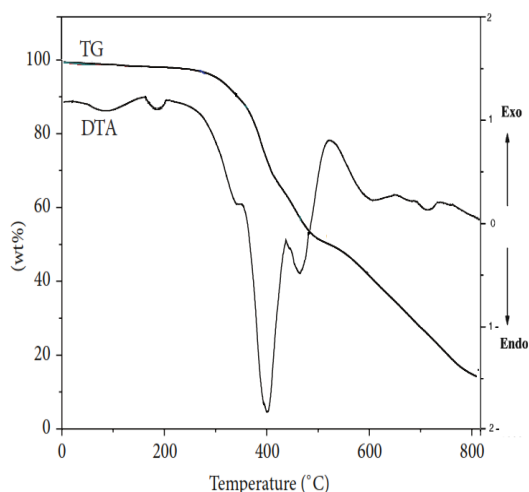


Figure 4 TG-DTA curve of (PFBN)

### 3.1.5 Thermal degradation of $C_{Fn2}$

TG-DTA curves for the  $C_{Fn2}$  LDH would indicated over Figure 5. Simultaneous thermogravimetric and differential thermal analysis (TG-DTA) measurements were performed for the precursor LDH. Powder has been heated from 25 °C to 1000°C at 10°C min<sup>-1</sup> under nitrogen purge. Five stages of mass loss would be watched over TG curve. The first thermal event in the temperature range of 25–120°C have been the mass loss of about 6%, which could be identified to the removal of surface-adsorbed and layer-intercalated water (dehydration of the sample), accompanied by an endothermic peak in DTA curve. The endothermic process plays an important role in the flame-retardant property, through the cooling of substrate to a temperature below that required to sustain the combustion process. The two exothermic peaks in DTA curve between 117 and 269°C were attributed to the decomposition of nitrate anions between the layers (11% mass loss) furthermore start of cobalt ferrite crystallization. The other two events between 269 and 600°C were allocated to the loss of structural water (the removal of hydroxylation in LDH layers). Over 600°C no weight loss has been observed and the crystallization process was finished. An expansive endothermic event was observed in DTA curve between 600 and 900°C refers to the densification of the powder.

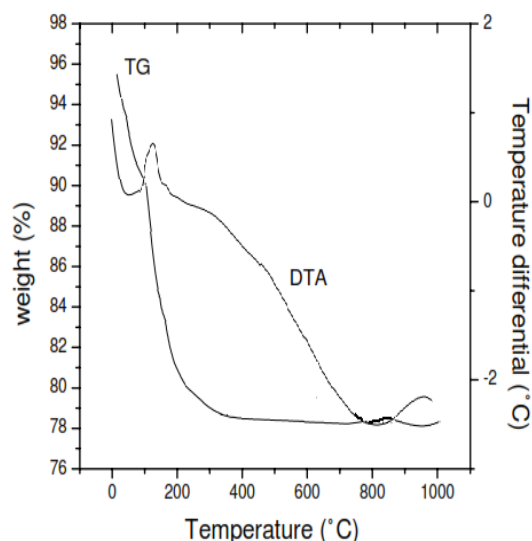


Figure 5 TG-DTA curve of LDH ( $C_{Fn2}$ )

### 3.1.6 Thermal degradation of $C_{Fn1}$

$C_{Fn1}$  sample (10mg) were loaded into TG/DTA instrument and heated from 25 °C to 1000 °C at 10°C/min under Nitrogen flow. TG-DTA curves for ( $C_{Fn1}$ ) are demonstrated to Figure 6. On the TG curve, the hydrous compound suffers slow mass losses (1.54%) before 300 °C, which owing to desorption of physically adsorbed water. After that, the change of mass was caused by the loss of crystal

water; this process is corresponding to loss of water of crystallization through condensation of B–OH groups, giving birth to the substantially amorphous composition of  $2\text{ZnO}\cdot 3\text{B}_2\text{O}_3\cdot 7\text{H}_2\text{O}$ . Upon heating, sample suffers a pronounced mass loss step (10.95%) which occurs in the region of 410–580 °C, accompanied by an endothermic peak in DTA curve observed near 510 °C, which can be attributed to the dehydration of molecular water of crystallization. This dehydration temperature is acceptable for flame retardant additives to enhance flame-retardant properties. The endothermic process plays an important role in the flame-retardant property, through cooling the substrate to a temperature below that required to sustain the combustion process. At the temperature between 650 and 720 °C, there is an exothermic behavior related to crystallization of two anhydrous zinc borate phases,  $3\text{ZnO}\cdot 2\text{B}_2\text{O}_3$  and  $4\text{ZnO}\cdot 3\text{B}_2\text{O}_3$ . Along with heating,  $3\text{ZnO}\cdot 2\text{B}_2\text{O}_3$  turns to a liquid and crystalline  $4\text{ZnO}\cdot 3\text{B}_2\text{O}_3$  completely, which might a chance to be watched around 890 °C. Finally,  $4\text{ZnO}\cdot 3\text{B}_2\text{O}_3$  melts around 960°C.

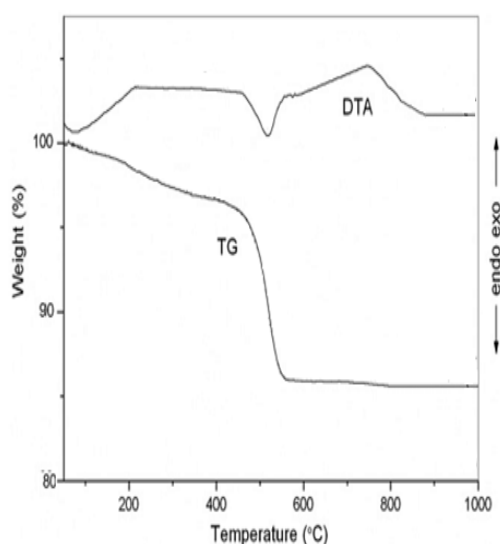


Figure 6 TG-DTA curve of ( $C_{Fn1}$ )

### 3.1.7 Thermal degradation of IFR-F3

DTA curve of IFR-F3 nano-coating is presented in Figure 7. PPA as a catalytic agent begins to decompose and liberate phosphoric acid at temperatures around 260 °C, and phosphoric acid further dehydrates to form pyrophosphate and polyphosphate at temperatures around 300 °C. The resulting acid takes part in the dehydration of PER furthermore PFBN through acid attack and esterification. Esterification between polyphosphate and PER leads to the formation of a fused carbonaceous material, and at the same time nonflammable gases such as ( $\text{NH}_3$ ,  $\text{CO}_2$  and  $\text{H}_2\text{O}$ ), released by MEL, might be better covered by this structure. PPA and MEL cause the fused

carbonaceous material to swell and form an intumescent char structure. The Diels–Alder reaction accompanied by ester pyrolysis prompts an aromatized structure. Repetition of these steps can eventually build up the carbonaceous char.<sup>22</sup> Throughout the formation of carbonaceous char, the acid assumes the greater imperative part which act as the catalyst of the dehydration process. The phosphoric acid generated on heating presumably reacts with Bentonite to form silicoaluminophosphate (SAPO) Figure 8.<sup>23-27</sup> SAPO is a promising solid acidic catalyst and might improve the acid source (phosphoric acid). The interaction of PPA, PER, MEL and PFBN causes an endothermic peak at 200–410 °C. The intumescent char formed from IFR-F3 nano-coating contributes an important fire protection to the underlying substrate.<sup>28-29</sup>

At the temperature higher than 550 °C, the intumescent char formed from the reaction of PPA, PER and PFBN is bit by bit oxidized. The oxidation process demonstrates an exothermic peak at 550–600 °C. After the exothermic peak, DTA curve forms a plateau at 610–760 °C, in which the oxidation trend is suppressed because of the presence of the inorganic protective materials. The reaction of Zinc Borate and ES in IFR F3 nano-coating at acid catalyzed reaction can form a zinc silicate polymer (ZSP). The ZSP in nano-coating transform and melt at a high temperature, as a blowing agent, causes the fused system to swell at the temperature higher than 750 °C, which provides for a further fire protection for the underlying substrate. ZSP Si–O–Si protective layer on the surface of residue insulating materials, also perform the fire retardant action. This silica layer slows down the diffusion of fire to underlying substrate and also serves to protect the substrate from heat and fire.<sup>30-31</sup> PPA and/or its degradation product contained in the coated effectively react with borate and/or boron oxide to yield borophosphate Figure 9.<sup>32</sup>

TG curve of IFR-F3 nano-coating is illustrated in Figure 7. A mass loss of 2.38% at 50–110 °C can be attributed to initial elimination of water. A mass loss of 10.21% at 200–410 °C corresponds to thermal degradation and interaction of PPA, PER, MEL and PFBN. A mass loss of 10.42% at 410–550 °C for the thermal decomposition of diphenyl ether linkages, and a mass loss of 2.16% at 550–610 °C is due to thermal oxidation of char layer. When the temperature is higher over 820 °C, there is no mass loss. The mass losses at 50–110 °C, 200–410 °C, 410–550 °C furthermore 550–600 °C initiates intumescence of IFR-F3 nano-coating.

In addition, the IFR-F3 has a high residue char of 50.21 wt% at 900°C and three characteristic weight-loss stages. The first characteristic

degradation stage shows up during 200–410°C, which will be the vast majority vital stage for intumescent char formation. This might be joined of the condensation reactions of *PFBN*, the self-condensation reaction of phosphoric acid what's more catalytic dehydration of polyphosphoric acid. The existence of polyphosphoric acid might catalyze *PFBN* to form diphenyl ether linkages. The second weight-loss stage around 410-550°C might be attributed of the thermal decomposition of diphenyl ether linkages which prompts the formation of the polyaromatic system at high temperature. The third step around 550°C is attributed to the thermal degradation of polyaromatic system. What is more, another DTA peak is clearly watched during 410-550°C, which don't exist over DTA curve of *PFBN*. The reason might be a chance to be that polyphosphoric acid can catalyze *PFBN* to form much more diphenyl ether linkages throughout the heating process. The thermal decomposition of a huge amount of diphenyl ether linkages at 410-550°C will be helpful for formation of char layer which could move forward the flame retardancy of *IFR-F3* system. For *IFR-F3*, the characteristic degradation stage 200 – 410°C of *IFR-F3* diminished over *PFBN* 300 – 450°C but improved the thermal stability at high temperature. The char yield of the *IFR-F3* composite might achieve 51.21 wt% at 900°C. Those motivation behind ought further bolstering a chance to be the outcomes of the thermal degradation of *PFBN* at the lower temperature what's more formation of intact char layer which can protect the remaining polymer from the heat of combustion, limit the access of oxygen to the polymer. Those non-flammable gases can dilute the concentration of oxygen what's more fuel, after that enhancing the flame retardancy.

TG- DTA analysis demonstrates that *IFR-F3* nano-coating decomposes, absorbs heat, swells and forms the porous protective materials during the different temperature ranges, and henceforth these cooperated reactions provide a good fire protection for the metallic substrate in a fire.

Summarizing, as stated by those over investigation about TG-TDA curves, a possible char-forming mechanism of *IFR* might be represented in Scheme 1.

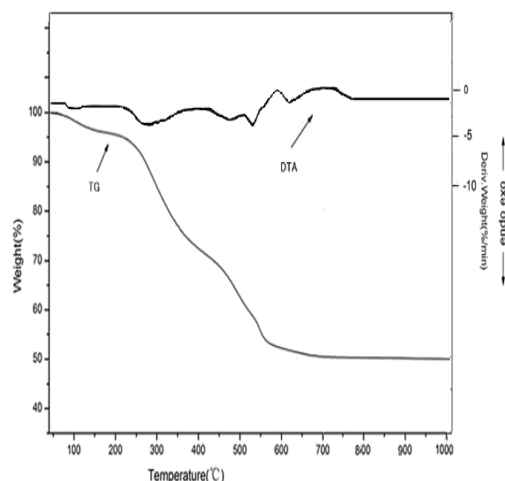


Figure 7 TG-DTA curves of (*IFR-F3*)

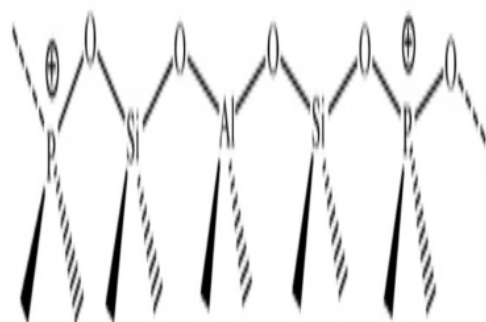


Figure 8 Silicoaluminophosphate (*SAPO*) structure.

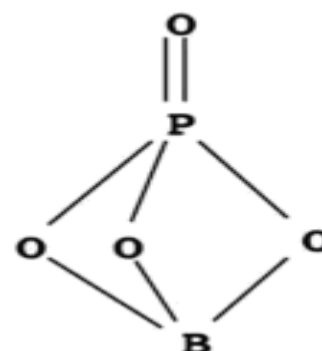


Figure 9 Borophosphate (*BPO4*) Structure.

### 3.2 Fire performance test

In the vicinity of a fire, the exposure of steel structure to high temperature reduces the strength and rigidity of steel also at last prompts steel structural collapse when the structure critical temperature is reached. Steel is a non-combustible material which exhibits a great ductility yet it starts will lose its structural properties between 470 and 500°C.<sup>33</sup> The steel structural safety in a fire can make guaranteed when the temperature of steel structural members stays under the structural critical temperature. The

temperature to scene of a fire will expand to 700°C within 10 min. At the fire temperature, inner temperature of exposed steel structure will increase to 500 °C and get to its critical strength after several minutes. Fast-falling mechanical property of steel at the high temperature prompts poor fire-resistant property of steel structure. Standard curve of temperature increment (ISO-834)<sup>17</sup> as represented by Figure 10 and Equation 2 is utilized likewise an reference of fire scene temperature. Its formula is demonstrated as below:

$$T - T_0 = 345 \log(8t + 1) \quad (2)$$

Where,  $T$  will be the flame temperature (°C),  $T_0$  the environment temperature at the starting of experiment (°C) and  $t$  the experimental time (min).

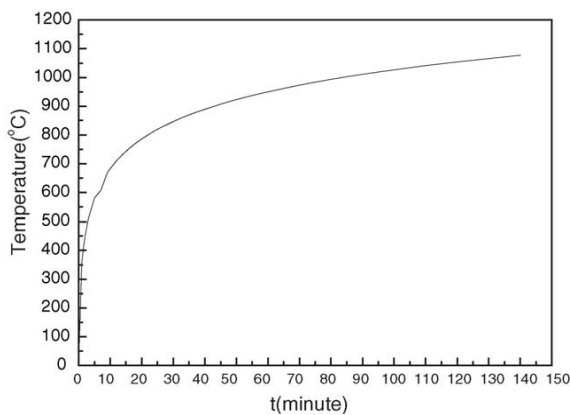


Figure 10 Standard curve of temperature increase (ISO-834).

The fire protection curves furthermore data of coatings are represented in Figure 11 also Table 2. The thickness of the intumescent protective layer of *IFR-F2* and *IFR-F3* nano-coatings is 43.9 and 62.4 mm, respectively, also their relative fire-resistant time is >120 min. The “foam” layer formed from *IFR-F1* coating has a low expanding time also can't provide good heat insulation for the metal substrate, something like that the fire-resistant time of *IFR-F1* coating is only 6 min. The “foam” layer, intumescent char formed from *IFR-F2* what's more *IFR-F3* nano-coatings could furnish a phenomenal fire protection for metal substrate. Therefore, the fire-resistant time and expanding times of *IFR-F2* furthermore *IFR-F3* nano-coatings will be superior to those of *IFR-F1* coating. ZSP particles have a high thermal stability at

high temperature also structure a Si–O–Si network inside the protective materials. A result those Si–O–Si network might protect the insulating materials at high temperature also might provide a mechanical reinforcement of the protective. In the intumescent process, two aspects must make investigated carefully: the chemical aspect and the physical aspect.<sup>34</sup> It will be fundamental the point when those intumescent coating degrades to form a thermally stable material as a result this material will protect the substrate from the fire. However, it will be additionally vital that the thermally stable material displays a barrier impact to heat furthermore to gases. So as will accomplish this effect, a foamed charred layer has to be formed. A moderate dissemination of gases in the structure throughout those intumescence permits the formation of an expanded structure concerning illustration in Figure 12. This will be not attained if the viscosity of the material is too high (which prompts a break of the layer) alternately too low (which prompts gases evolution to feed the flame). The vitality of both chemical and physical aspects is demonstrated by the moderate swelling and char formation. A potential char-forming mechanism of *IFR* will be quelled for Scheme 1.

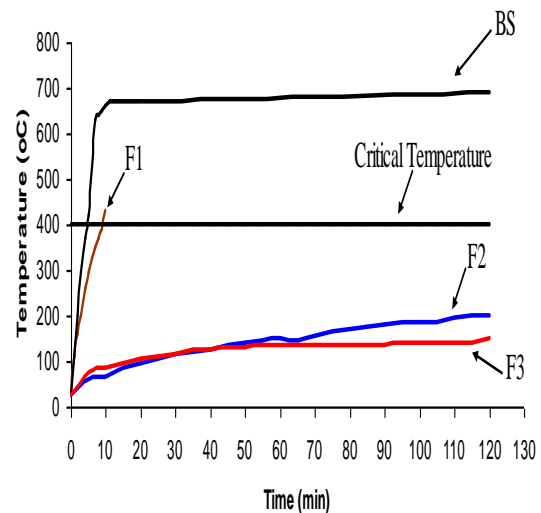


Figure 11 Time-temperature profile curves of bare steel plate (BS), *IFR-F1* (F1), *IFR-F2* (F2) and *IFR-F3* (F3).

Table 2 Data of fire protection properties of *IFR* coatings.

Coating	Thickness of char layer (mm)	Equilibrium temperature of coating (°C)	Fire-resistant time (min)	Intumescent-rate
<b>IFR-F1</b>	- <sup>a</sup>	>Critical temperature	6	- <sup>a</sup>
<b>IFR-F2</b>	43.9	198.2	>120	21.7
<b>IFR-F3</b>	62.4	150.4	>120	31.2

<sup>a</sup> The coating did not adhere to the steel plate during test.

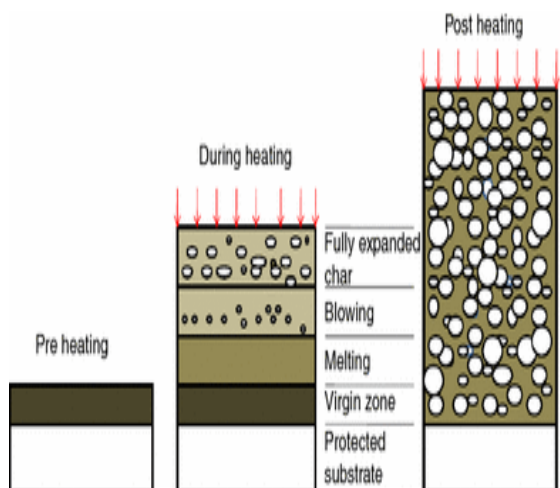


Figure 12 Schematic representation of intumescence process.



Figure 15 The steel plate coated with IFR-F3 during the fire performance test.

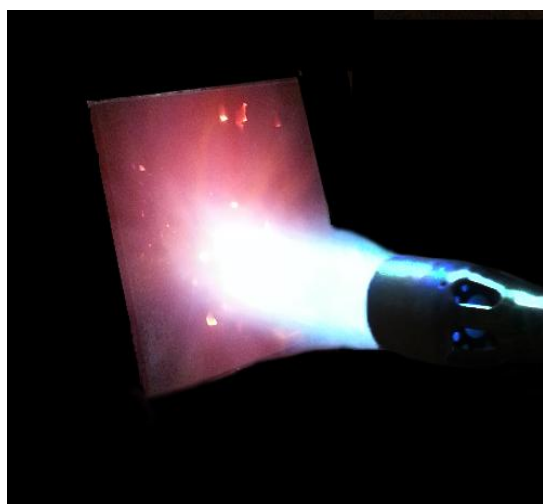


Figure 13 The bare steel plate during the fire performance test.



Figure 14 The steel plate coated with IFR-F2 during the fire performance test.

### 3.3 Anticorrosion property test

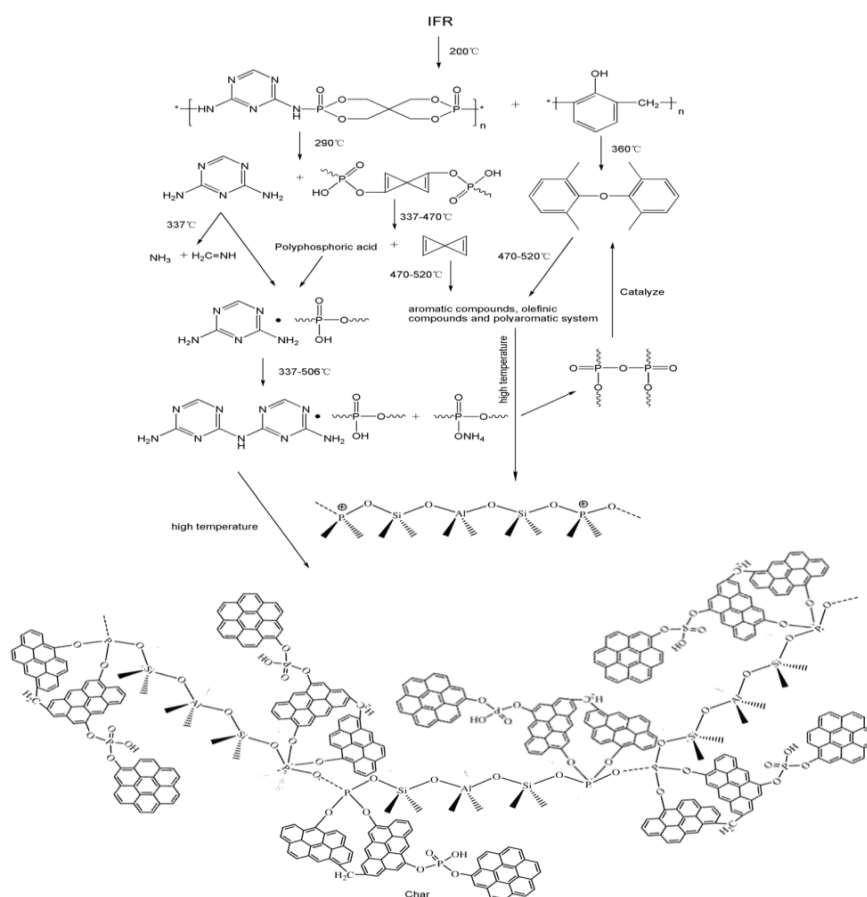
Anticorrosion property of flame-retardant coatings has been confirmed utilizing salt spray resistance test. In the salt spray chamber the specimens were put meeting those taking after conditions:

- (i) Every last one of specimens was underpinned parallel of the central heading for level stream of fog.
- (ii) Specimens holders have been committed of plastic and, therefore, specimens were not in contact with one another alternately worth at whatever worth any metallic material.
- (iii) A 5% solution of sodium chloride has been atomized by compressed air in the chamber.
- (iv) Temperature of the chamber has been held in 38°C (100°F).

Specimens were laid open under above-mentioned conditions at different time intervals up to 1100 hour. After the required exposure period, the specimens were inspected as per ASTM D1654-08(2016) (Standard Test Method for Evaluation of Painted or Coated Specimens Subjected to Corrosive Environments). This method provides a means for assessing and comparing basic corrosion performance of substrate, pretreatment, alternately coating system, or combination. Thereof, then afterward exposure to corrosive environment, the specimens were deliberately uprooted from the holder what's more delicately washed in clean running water, to uproot salt deposits from their surfaces, and then instantly dried. Exposed surface at the scribes have been cleaned with brush to uproot every last one of rust. Mean creepage starting with those scribe and failed area have been measured also rated as per ASTM D1654-08(2016). Similarly, estimations were likewise conveyed out for the blisters showed up for scribed and unscribed sides.

Specimens with furthermore without scribe exposed to the salt fog were assessed with respect to mean creepage (from scribe) also blistering. Table 3

summarizes the salt spray effects for IFR-F1, IFR-F2 furthermore IFR-F3 coatings.



Scheme 1 Suggested Schematic representation of Char-forming mechanism of IFR.

Table 3 Salt Spray Test Results: Mean Creepage from Scribe (mm), % Area Failed from Unscribe

Coating System	Mean Creepage from scribe (mm)		Unscribed	
	Millimeters	Rating Number	% Area Failed	Rating Number
IFR-F1	Over 16.0	0	85	0
IFR-F2	1.45	7	5	7
IFR-F3	1.38	7	4	7

### 3.4 Resistance to freeze–thaw cycle

Freeze-thaw cycle testing is a part of stability testing that permits figuring out in those formulas will stay stable under different states. This type of test puts sample through a series of extreme, rapid temperature progressions that it might experience throughout ordinary processes. The stability of flam-retardant coatings has been confirmed utilizing resistance to freeze–thaw cycle. Those effects are recorded for Table 4. The resistance to freeze–thaw cycle of IFR-F1 coating is only 2 times, and cracking-off. The resistance to freeze–thaw cycle of IFR-F2 nano-coating is 24 times, whereas the resistance to freeze–thaw cycle of IFR-F3 nano-coating is 26 times.

Table 4 Data of the resistance to freeze–thaw cycle

Coating System	IFR-F1	IFR-F2	IFR-F3
Resistance to freeze–thaw cycle (times)	2	24	26

## IV. CONCLUSION

The target of this effort has been with investigation of that effectiveness of different intumescent formulations, designed for the protection of steel in the off chance of a fire. Utilizing the fire performance test, it will be ascribed that the intumescent char from the three flame retardant additives PPA/MEL/PER alone is light and crumbly, bringing about the detachment of the char segregated

from the plate throughout those test. However, the adhesion of the coating to the steel plate indicated improvement for *IFR-F2* flame retardant, which furnished longerlasting protection. The *IFR-F3* flame retardant indicated the best fire protection as far as thermal stability, expansion of char layer, surface structure.

It may be indicated that intumescent behaviour might a chance to be imparted to polymers by means of suitable additives. Fire-retardant polymeric materials characterized by reduced overall fire hazard as far as amount, obscuring power furthermore toxicity of smokes evolved on burning can undoubtedly be prepared. The *IFR-F1* coating cannot provide beneficial fire protection for the metallic substrate. The *IFR-F2* and *IFR-F3* nano-coatings can form useful intumescent char also subsequently provides an improved fire resistance. The fire performance, anticorrosion, thermal stability what's more resistance to freeze–thaw cycle properties of the *IFR-F1* flame retardant coating are badly, while the great fire performance, anticorrosion, thermal stability and resistance to freeze–thaw cycle properties of *IFR-F2* and *IFR-F3* flame retardant nano-coatings. A synergistic impact has been found between *PFBN* and bentonite which improved thermal stability and flame retardancy. The phosphoric acid generated on heating probably reacts with bentonite to form silicoaluminophosphate (SAPO).

From the thermal degradation studies of intumescent flame retardants, conclusion a chance to be draw that the mechanism of intumescence generally comprises of five steps: (i) the catalyst (acid source) decomposes to form mineral acid, (ii) those resultant acid reacts with the carbonific to form esters by dehydration reaction, (iii) the ester decomposes to form an expansive volume of carbon and then releases the acid, (iv) the resinous material melts to form a film alternately skin over the carbonaceous material, what's more (v) the blowing agent release gases strained in the melted matrix making it swell what's more shaping an insulating multi-cellular protective char layer also causing the carbon to foam, forming a thick, exceptionally effective insulation. This carbonaceous char shield restricts the transfer of heat from the source to the substrate what's more keeps further degradation of the underlying material. The succession of the intumescence process also reactions can be summarized as takes after:

1. Softening and melting of the polymeric binder.
2. Discharging of inorganic acids.
3. Carbonization of char formers.
4. Discharge of gaseous products by blowing agenize.
5. Foaming also expansion of the mixture.
6. Crosslinking also solidification of char.

Salt spray resistance test, fire performance test uncover that *PPA/MEL/PER* coating is defenseless against corrosives and subsequently the fire resistance will be extremely hurt to corrosive environment, while *IFR-F2* furthermore *IFR-F3* nano-coatings show extraordinary corrosive resistance what's more fire-retardancy.

#### REFERENCES

- [1]. J.A. Rhys, Intumescent coatings and their uses, *Fire Mater.* 4, (1980), 154-156.
- [2]. WS. Mardis Organoclay rheological additives: past, present and future, *Journal of the American Oil Chemists' Society*, 61, (1984), 382-387.
- [3]. M. Jimenez, S. Duquesne, S. Bourbigot, Intumescent fire protective coating: toward a better understanding of their mechanism of action, *Thermochimica Acta*, 449, (2006), 16-26.
- [4]. Duquesne S., Magnet S., Jama C., Delobel R., Intumescent paints: fire protective coatings for metallic substrates, *Surface and Coatings Technology*, 302, (2004), 180–181.
- [5]. Wladyka-Przybylak M., Kozłowski R., The thermal characteristics of different intumescent coatings, *Fire and Materials*, 23 (1), (1999), 33-43. S.
- [6]. Duquesne, S. Magnet, C. Jama, R. Delobel, Thermoplastic resins for thin filmintumescent coatings- towards a better understanding of their effect onintumescence efficiency, *Polymer Degradation and Stability*, 88, (2005), 63-69.
- [7]. B. Ostman, A. Voss, A. Hughes, P.J. Hovde, Q. Grexa, Durability of Fire Retardant Treated Wood Products at Humid and Exterior Conditions Review of literature, *Fire and Materials*, 25 (3), (2001), 95-104.
- [8]. Z.Y. Wang, E.H. Han, W. Ke, Influence of expandable graphite on fire resistance and water resistance of flame-retardant coatings, *Corrosion Science*, 49 (5), (2007), 2237-2253.
- [9]. W. Funke, Problems and progress in organic coatings science and technology, progress in organic coatings, 31, (1997), 5-9.
- [10]. W. Funke, Thin-layer technology in organic coatings, progress in organic coatings, 28 (1), (1996), 3-7.
- [11]. M.N. Sathyanarayana, M. Yaseen, progress in organic coatings, 26, (1995), 275-313.
- [12]. J.H. Koo, W. Wootan, W.K. Chow, H.W. Au Yeung, S. Venumbaka, Flammability Studies of Fire Retardant Coatings on Wood,” *Fire and Polymers: Materials and Solutions for Hazard Prevention*, G.L. Nelson and C.A. Wilkie, eds.,

- Fire and Polymers, ACS Symposium Series No.797, (2001), 361–374.
- [13]. R. Delobel, M. LeBras, N. Ouassou, F. Alistiqa, Thermal behaviors of ammonium polyphosphate-pentaerythritol and ammonium pyrophosphate-pentaerythritol intumescent additives in polypropylene formulations, *J Fire Science*, 8, (1990), 85-99.
- [14]. G. Hernández-Padrón, M. García-Garduño, M.A. Canseco, V.M. Castaño, Nanoparticles-Based Phenol-Formaldehyde Hybrid Resins, *Journal of Nanoscience and Nanotechnology*, 8, (2008), 3142-3145.
- [15]. Guo Yonghe, A kind of anti - corrosion phenolic resin compression coating, CN Patent No. CN 103421427 A (2013).
- [16]. S. J. Rajendra, M. Vishal , V. B. Avinash, G. H. Dilip, M.P. W. Pramod, Gulzar, Synthesis of multicore phenol formaldehyde microcapsules and their application in polyurethane paint formulation for self-healing anticorrosive coating, *International Journal of Industrial Chemistry*, (2013), 4:31.
- [17]. International Standardization for Organization - Fire Resistance Test - Elements of Building Construction, ISO, vol. 834, Geneve, 1994.
- [18]. MC. Yew, NH. Ramli, Investigation on fire protection of intumescent coatings for steel. In: *Proceedings of 1st international seminar on sustainable infrastructure and building environment in developing countries (SIBE 2009)*. Bandung, Indonesia; 2009.
- [19]. M. C. Yew, S.N.H. Ramli, Fire-resistive performance of intumescent flame-retardant coatings for steel, *Materials and Design*, 34, (2012), 719–724.
- [20]. W. Guojian, Y. Jiayun, Influences of binder on fire protection and anticorrosion properties of intumescent fire resistive coating for steel structure, *Surface & Coatings Technology*, 204, (2010), 1186–1192.
- [21]. W. Zhenyu, H. Enhou, K. Wei, An investigation into fire protection and water resistance of intumescent nano-coatings, *Surf. Coat. Tech.*, 201, (2006), 1528– 1535.
- [22]. A.R. Horrocks, D. Price, 2001. *Fire retardant materials*. Woodhead Publishing/ CRC Press.
- [23]. M. Haiyun, T. Lifang, X. Zhongbin, F. Zhengping, Intumescent flame retardant-montmorillonite synergism in ABS nanocomposites, *Applied Clay Science*, 42 (1-2), (2008), 238– 245.
- [24]. J.A. Martens, P.J. Grobet, P.A. Jacobs, Catalytic activity and Si, Al, P ordering in microporous silicoaluminophosphates of the SAPO-5, SAPO-11, and SAPO-37 type, *Journal of Catalysis*, 126 (1), (1990), 299-305.
- [25]. H.Y. Ma, Z.P. Fang, L.F. Tong, Preferential melt intercalation of clay in ABS/brominated epoxy resin/antimony oxide (BEReAO) nanocomposites and its synergistic effect on thermal degradation and combustion behavior, *Polymer Degradation and Stability*, 91, (2006), 1972–1979.
- [26]. Y.F. Ma, Li. N. Ren, X.T. Xiang, S.H. Guan, Synthesis of SAPO-41 from a new reproducible route using H<sub>3</sub>PO<sub>3</sub> as the phosphorus source and its application in hydroisomerization of n-decane, *Journal of Molecular Catalysis A: Chemical*, 250 (1-2), (2006), 9–14.
- [27]. Z.L. Ma, W.Y. Zhang, X.Y. Liu, Using PA6 as a charring agent in intumescent polypropylene formulations based on carboxylated polypropylene compatibilizer and nano-montmorillonite synergistic agent, *Journal of applied polymer science*, 101 (1), (2006), 739–746.
- [28]. A. Reshetnikov Antonov, T. Rudakova, G. Aleksjuk, Some aspects of intumescent fire retardant systems, *Polymer Degradation and Stability*, 54 (2-3), (1996), 137-141.
- [29]. A.F. Yaylor, F.R. Sall, Thermal analysis of intumescent coatings, *European Polymers Paint Colour Journal*, 182 (4301), (1992), 122-130.
- [30]. L.G. Hanu, G.P. Simon, J. Mansouri, Development of polymer–ceramic composites for improved fire resistance, *Journal of Materials Processing Technology*, (153–154), (2004), 401-407.
- [31]. G. Leder, T. Ladwig, V. Valter, New effects of fumed silica in modern coatings, *Progress in Organic Coatings*, 45 (2-3), (2002), 139-144.
- [32]. R. Delobel, M. Le Bras, B. Mouchel, J.M. Leroy, *Ann. Compos.*, (1990), 3–12
- [33]. EN1994-1-2, "Design of composite steel and concrete structures." European Committee for Standardization, Brussels.
- [34]. C. G. Satish, S. Abhishek, S. Dheerender, G. Sandhya, Melamine Polyimide Composite Fire Resistant Intumescent Coatings, *Defence Science Journal*, 63, (4), (2013), 442-446.

A. Nour El-Dein. " Fire-Resistivity Personification Of Waterborne Intumescent flame-Retardant Nano-Coatings For Steel Structures: Application." *International Journal of Engineering Research and Applications (IJERA)*, vol. 7, no. 8, 2017, pp. 01–12.